

RTMap: Real-Time Recursive Mapping with Change Detection and Localization

Yuheng Du^{1,†} Sheng Yang^{1,†,✉} Lingxuan Wang¹ Zhenghua Hou¹ Chengying Cai¹
 Zhitao Tan¹ Mingxia Chen¹ Shi-Sheng Huang² Qiang Li¹
¹Unmanned Vehicle Dept., CaiNiao Inc., Alibaba Group ²Beijing Normal University
 {guofan.dyh, shengyang}@cainiao.com

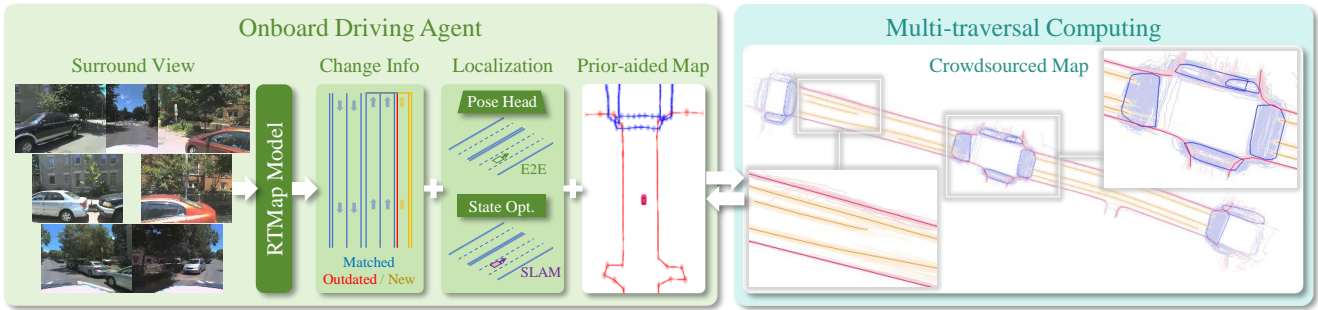


Figure 1. RTMap performs real-time online HD mapping on onboard driving agents, simultaneously solving map-based localization, map change detection, and online map fusion tasks. Meanwhile, a cloud service asynchronously stitches crowdsourced online HD maps into a global prior-map for subsequent traverses.

Abstract

While recent online HD mapping methods relieve burdened offline pipelines and solve map freshness, they remain limited by perceptual inaccuracies, occlusion in dense traffic, and an inability to fuse multi-agent observations. We propose RTMap to enhance these single-traversal methods by persistently crowdsourcing a multi-traversal HD map as a self-evolutional memory. On onboard agents, RTMap simultaneously addresses three core challenges in an end-to-end fashion: (1) Uncertainty-aware positional modeling for HD map elements, (2) probabilistic-aware localization w.r.t. the crowdsourced prior-map, and (3) real-time detection for possible road structural changes. Experiments on several public autonomous driving datasets demonstrate our solid performance on both the prior-aided map quality and the localization accuracy, demonstrating our effectiveness of robustly serving downstream prediction and planning modules while gradually improving the accuracy and freshness of the crowdsourced prior-map asynchronously. Our source-code will be made publicly available at <https://github.com/CN-ADLab/RTMap>.

†: Equally contributed. ✉: Corresponding author.

1. Introduction

High-Definition (HD) maps enriched with geometric, semantic, and behavioral annotations, are foundational to autonomous driving systems – enabling robust obstacle avoidance, centimeter-level parking precision, and customized driving policies. As highlighted in a recent survey [33], the field has shifted from reliance on costly offline mapping pipelines to online HD mapping [23–25], which generates maps in real-time using consumer-grade sensors and embedded computing resources. These methods empower vehicles to simultaneously perceive and construct HD maps onboard, unlocking a dual-mode Operational Design Domain (ODD): (1) *First-Traversal Autonomy*: In unexplored environments, vehicles operate without a prior-map, leveraging real-time perception for basic autonomy, e.g., Lane Centering Control (LCC) and Autonomous Emergency Braking (AEB). (2) *Crowdsourced Enhancement*: Once aggregated from multi-agent traversals, such fused prior-maps can provide previous perceptual knowledge to extend sensing range, resolve occlusions, and elevate autonomy to L4 standards, e.g., dense urban navigation and unprotected left turns.

While the community rapidly evolves methods and strategies for the first-traversal autonomy [33], *crowdsourced enhancement* remains under-explored following

such a shifted architecture. Revisiting online HD mapping frameworks [23–25], most of them treat mapping as a single-pass process, failing to effectively utilize the rich contextual knowledge available from multiple traversals of the same scene. To fully harness this multi-traversal knowledge, two fundamental capabilities are essential: (1) precise localization within the prior-map to accurately align the current surroundings with existing spatial data, and (2) robust detection and adaptation to structural changes in road networks – such as lane modifications or construction zones – to maintain map freshness by eliminating outdated information. Although numerous studies have proposed effective methods to solve these problems independently [14, 30], these two sub-tasks and the overall prior-aided online HD mapping task essentially solve the retrieval, correspondence, and differentiation problems between multi-traversal map elements. To address these challenges, we propose RTMap with novel comprehensive query and matching, to solve the element identification and map association in a unified end-to-end framework for addressing all these tasks. Moreover, we further introduce an explicit modeling of the geometric uncertainty of extracted map elements, to facilitate both a probabilistic-aware state estimation of the 6 degrees of freedom (DOF) vehicle poses and noise-aware multi-traversal prior-map fusion. Thus, we lead to highly accurate real-time HD mapping, especially suitable for autonomous driving scenarios.

In summary, our RTMap offers three key contributions:

- The first end-to-end framework supports multi-traversal online HD mapping while simultaneously addressing map-based localization and change detection to robustly and stably serve downstream autonomous driving modules.
- By quantitatively inferencing the probabilistic density of perceived vectorized HD map elements, RTMap further improves localization accuracy through end-to-end learning and explicit state estimation.
- RTMap proposes a crowdsourcing mechanism to recursively update the offline prior-map asynchronously. The inferenced probabilistic density and change information further improve the accuracy of the prior-aided online HD map.

Experiments on localization, mapping, and map change detection tasks on multiple publicly available datasets [3, 17] have demonstrated our effectiveness in simultaneously addressing them through an end-to-end framework. We will release our labeled assets on these datasets and our multi-task model to facilitate future research.

2. Related Work

In decades, offline mapping pipelines [32, 38] have become the mainstream for mass-producing HD maps [10]. Once

these maps are constructed, centimeter-level map-based localization deployed onboard can accurately fetch and transform these map elements for downstream prediction and planning tasks. However, recent advances [33] in onboard real-time HD mapping are deeply reforming the solution of mapping (Sec. 2.1) and localization (Sec. 2.2).

2.1. Online HD Mapping

Single-traversal single moment methods. HDMapNet [19] and MapTR [23, 24] use the encoder-decoder paradigm to transform sensor input into a unified Bird’s Eye View (BEV) representation and output an explicit local HD map. VectorMapNet [26] aggregates features generated from different modalities into a common BEV feature space for multi-sensor mapping. GKT [7] leverages calibrated camera parameters to determine the correspondence between 2D positions and BEV grids for constructing full correlations. LaneSegNet [21] proposes a heads-to-regions mechanism for capturing long-range attention and an identical initialization strategy for enhancing the learning of positional priors for lane attention.

Single-traversal temporal fusion methods. To facilitate the stability of online HD mapping between consecutive frames, many subsequent methods [20, 39] leverage BEVFormer [22] for temporal self-attention to fuse temporally adjacent BEV information recurrently. Other explicit methods [6] use odometry to transform perceived results and perform voxel mapping for multi-frame fusion.

Prior-aided methods. Previous works [1, 31] demonstrate that prior-informed online mapping can further improve completeness and stability. Unlike the single-traversal methods mentioned above, prior-aided methods require both localization and change detection to establish correct correspondences between maps. We mainly found two categories of prior-aided methods for online HD mapping: The first category [35, 37] uses neural representation as prior-maps, which requires dense storage unsuitable for mass production, and it is also not intuitive for quality inspection and manual correction. The second category uses Standard-Definition (SD) or HD maps as prior knowledge: SMERF [27] queries the SD map at the ego vehicle’s location for lane-topology reasoning, and U-BEV [4] extracts BEV features from both sensors and SD map to reach meters-level accuracy through template matching. P-MapNet [16] leverages SD priors for coarse localization and HD priors for final map refinement. Our method belongs to the latter category, stepping further to reach real-time centimeter-level localization accuracy beyond previous methods through an end-to-end model. Meanwhile, RTMap manages to self-enclose the maintenance of prior HD maps, inferencing the probabilistic density of online HD map elements for noise-aware HD crowdsourcing.

Change detection. Considering possible road structural

changes, recent methods such as ExelMap [34] add additional heads for detecting element-wise insertion and deletion events. Also, recent advances for offline pipelines [36] leverage prior-map encoding and unify the feature space for the predicted and historical instances using distinct multi-layer perceptron (MLP) networks to associate and pick up changed instances. Compared to these methods, our method operates onboard and thus instantly serves downstream tasks without relying on engineering practices to ensure the refreshed HD map is efficiently deployed.

2.2. Map-based Localization

Online HD mapping reforms localization separately into odometry [18, 41] for temporal reasoning and map-based localization [8, 28] for aggregating prior knowledge if such prior exists. We found several learning-based methods contain similar architectures above but are individually designed for map positioning tasks: BEV-Locator [40] adopts the transformer structure in cross-modal feature association to address cross-modality matching between semantic map elements and camera images. EgoVM [14] designs learnable embeddings and a transformer decoder to bridge the representation gap between vectorized HD maps and sensor BEV features to reach centimeter-level localization accuracy. However, these methods treat localization as an isolated task and still require a standalone HD mapping progress for referring to. Considering the main objective of a precise map-based localization – better aggregating prior knowledge for map servicing, we choose to union the localization task with all related tasks that may influence its accuracy – online map prediction accuracy, road structural changes, erroneous map elements matching, and possible occlusions – and thus lean toward a multi-task end-to-end manner.

Meanwhile, inspired by Gu et al. [12], who additionally output uncertainty estimates for downstream prediction tasks, we contribute to introduce uncertainty as thorough information, which can either explicitly or implicitly improve the quality of localization and prior-aided mapping, enabling end-to-end architecture to optionally perform optimization-based state estimation as Simultaneous Localization and Mapping (SLAM) approaches [2, 5, 9, 15, 42] for interpretability while maintaining accuracy.

3. Methodology

3.1. Method Overview

Problem formulation. In the current traverse t given a single moment of multi-sensor frames \mathbf{I}_t (typically contains calibrated surround view camera frames) and a prior-map \mathcal{M}_{t-1} formed by previous multi-agent traverses, our end-to-end framework simultaneously addresses the following

tasks:

$$\begin{aligned} \{\mathbf{M}_t, \mathbf{U}_t, \mathbf{D}_t, \mathbf{T}_t^{\mathbb{E}}\} &\leftarrow \text{RTMapModel}(\mathbf{I}_t, \mathcal{M}_{t-1}), \\ \{\mathbf{T}_t^{\mathbb{R}}\} &\leftarrow \text{Localize}(\mathbf{M}_t, \mathbf{U}_t, \mathbf{D}_t, \mathcal{M}_{t-1}), \\ \{\mathcal{M}_t\} &\leftarrow \text{CSrc}(\mathbf{M}_t, \mathbf{U}_t, \mathbf{D}_t, \mathbf{T}_t, \mathcal{M}_{t-1}). \end{aligned} \quad (1)$$

As illustrated in Fig. 2, we use a multi-task onboard model $\text{RTMapModel}(\cdot)$ with hybrid queries (Sec. 3.2) and an existence-aware matching scheme (Sec. 3.3) to detect three classes of map elements: matched $\mathbf{M}_t^{\mathbb{M}}$, outdated $\mathbf{M}_t^{\mathbb{F}}$, and newly observed $\mathbf{M}_t^{\mathbb{N}}$. Therefore, we can separately infer possible map change events $\Delta_t \triangleq \{\mathbf{M}_t^{\mathbb{F}}, \mathbf{M}_t^{\mathbb{N}}\}$ besides matched elements $\mathbf{M}_t^{\mathbb{M}}$ to reduce their impact on localization and update the crowdsourced map afterward. We design our loss function (Sec. 3.4) for multiple additional tasks, jointly inferencing (1) the per-vertex probabilistic density \mathbf{U}_t of these map elements, (2) point-wise correspondences \mathbf{D}_t between re-observed and prior-map elements $\langle \mathbf{M}_t^{\mathbb{M}}, \mathcal{M}_{t-1} \rangle$, and (3) an end-to-end pose w.r.t. the prior-map $\mathbf{T}_t^{\mathbb{E}} \in \mathbb{SE}^3$. For explicitly addressing the 6-DOF localization if required, we also implement a state optimizer $\text{Localize}(\cdot)$ leveraging deducted correspondences \mathbf{D}_t for an optimization-based pose solution $\mathbf{T}_t^{\mathbb{R}} \in \mathbb{SE}^3$ as an option (Sec. 3.5). As $\mathbf{T}_t^{\mathbb{E}}$ and $\mathbf{T}_t^{\mathbb{R}}$ share the same purpose, we compare their performance (Tab. 4) and retain the estimator of $\mathbf{T}_t^{\mathbb{R}}$ for tightly coupling inertial measurements if necessary. Finally, $\text{CSrc}(\cdot)$ operates on-the-cloud to fuse multi-traversal inferences and update the crowdsourced map (Sec. 3.5). We use GPS measurements to provide a meters-level initial pose \mathbf{T}_t^0 for fetching a truncated local crowdsourced HD map \mathcal{M}_{t-1} for these onboard operations.

3.2. Hybrid Queries

To tackle the challenges of localization, mapping, and change detection concurrently, we propose hybrid queries enabling the network to process various query types and obtain matched, outdated, and newly observed elements to address all three tasks effectively. In this context, the decoder initially receives two types of queries $\mathbf{Q}_{\text{prior}}$ and \mathbf{Q}_{new} from prior-map embedding and sensor encoding, respectively. After training with query-based matching (Sec. 3.3), we further differentiate $\mathbf{Q}_{\text{prior}} \rightarrow \{\mathbf{Q}_{\text{map}}, \mathbf{Q}_{\text{fake}}\}$, with the first part \mathbf{Q}_{map} telling reliable correspondences for localization and the latter part \mathbf{Q}_{fake} specifying outdated elements.

Inspired by MapTR [23] and MapEX [31], we use unified representation to encode each $\mathbf{Q}_{\text{prior}}$ as an instance represented by fixed points, where the first two dimensions of each point are encoded as XOY coordinates, and the remaining N dimensions represent category information using one-hot encoding. Due to the characteristics of the transformer, the number of queries is fixed. Therefore, the remaining queries are designated as \mathbf{Q}_{new} padded with ze-

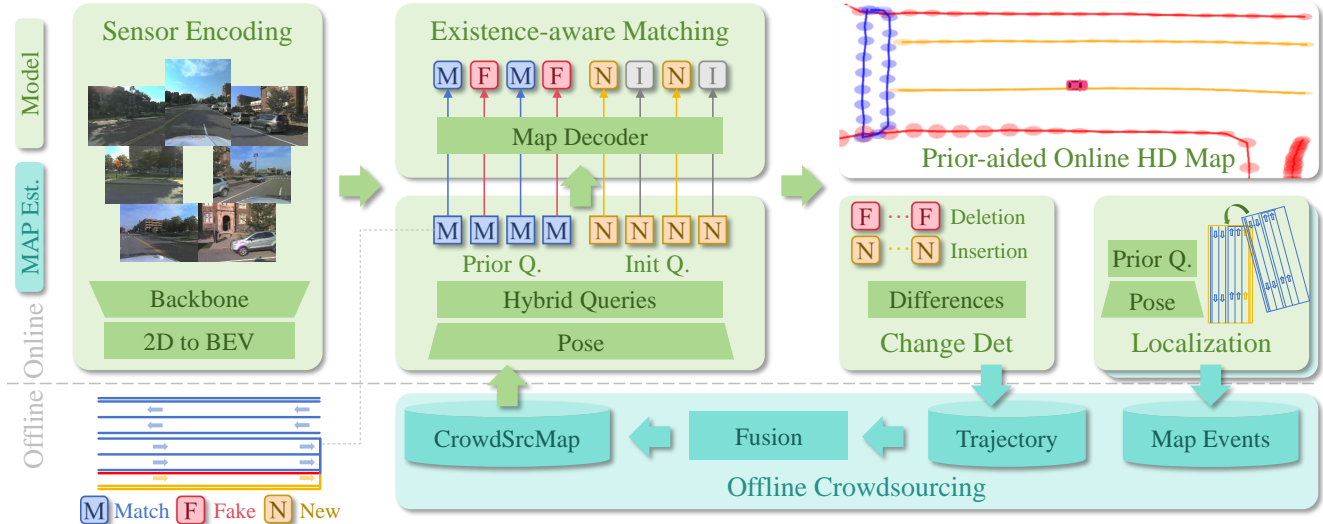


Figure 2. Online and offline modules of RTMap. We encode sensors and the crowdsourced HD map to perform hybrid queries and existence-aware matching to obtain matched, outdated, and newly observed HD map elements online. Matched queries can be used for either a pose head or a maximum a posteriori (MAP) state estimator for obtaining the 6-DOF vehicle poses. During offline, we gather multi-traversal local HD maps to fuse them to improve the accuracy and completeness of the crowdsourced map.

ros. Finally, after passing through a linear layer, these queries are combined with the hierarchical query embeddings Q_{hie} [23] to obtain the hybrid queries Q_{hybrid} formulated as follows:

$$Q_{hybrid} = \{Q_{map}, Q_{fake}, Q_{new}\} + Q_{hie}. \quad (2)$$

3.3. Existence-aware Matching

Matching in training. In contrast to MapEX [31], which leverages pre-attribution from ground truth for training, we need to tell Q_{fake} apart from Q_{map} for change detection and improving multi-task performances. Therefore, with the help of ground truth map-changing events, we choose to implement only a pre-attribution of Q_{map} predictions to their corresponding existing map elements. Besides, the remaining map elements are matched with Q_{new} predictions using conventional Hungarian matching.

As an observable consequence of the training process (Fig. 3), different types of queries exhibit distinct behaviors under this matching strategy. Due to pose perturbations, Map queries Q_{map} are projected near their actual locations. After that, their corresponding reference points gradually move to the correct positions. In contrast, since fake queries Q_{fake} do not exist in the prior-map, they lead to unstable behavior in their reference points. The rest of the new queries Q_{new} detect newly occurring elements from the current traverse.

Matching in inference. During the inference stage, without ground truth annotations, Q_{map} and Q_{fake} are mixed within the prior queries Q_{prior} . Since Q_{fake} were not pre-attributed during the training phase, the category confidence associ-

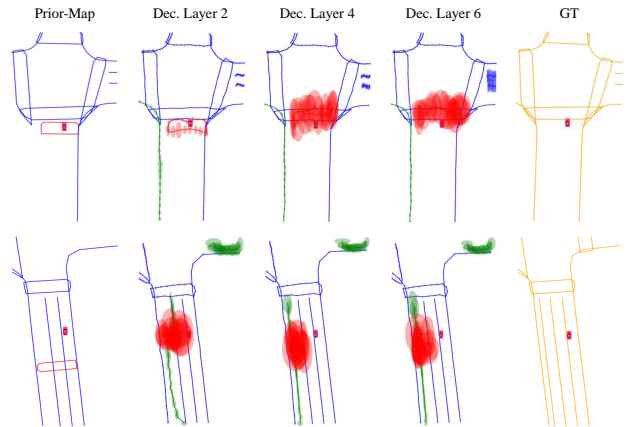


Figure 3. Trend of queries in different decoder layers. Q_{map} , Q_{fake} , Q_{new} are colorized in blue, red, and green, respectively. The ellipsoid reflects their uncertainty. Hence, outdated map elements are gradually filtered from matched map elements.

ated with Q_{fake} will be significantly lower than those for Q_{map} , providing strong evidence to differentiate between the two types of queries. Therefore, we believe that using the confidence score of the predictions corresponding to Q_{prior} can effectively distinguish between them.

3.4. Loss Function for Map Elements and Poses

Composite Geometric Loss for Element Vertices. Following Gu et al. [12], we choose two uni-variate Gaussian distributions to model map elements, allowing us to additionally output the probabilistic density U_t jointly with the

location \mathbf{M}_t of map element vertices. Specifically, we augment the vertex of each element with two standard deviations on the XOY plane, regarding them as horizontal 2D Gaussians for obtaining a probabilistic representation. For inferencing such additional information, we augment a negative log-likelihood (NLL) loss \mathbf{L}_{nll} for each vertex, as:

$$\begin{aligned} \mathbf{L}_{\text{pts}} &= \lambda_1 \cdot \mathbf{L}_{\text{nll}} + \lambda_2 \cdot \mathbf{L}_{\text{mht}}, \\ \mathbf{L}_{\text{nll}} &= \sum_{v=1}^V \sum_{k=1}^2 \left(\log(2\sigma_v^k) + \frac{|\mathbf{m}_v^k - \mu_v^k|}{\sigma_v^k} \right), \end{aligned} \quad (3)$$

where $\mathbf{m}|_{\text{xy}} \sim \mathcal{N}^2(\mu, \sigma)$ incorporates a 2D Gaussian distribution for each point’s XOY coordinate. We keep their Z-value representation unchanged due to insufficient observability. The parameters $\mu_v^k, \sigma_v^k \in \mathbb{R}$ denote the location and scale parameters of the k^{th} dimensional Gaussian distribution for a vertex \mathbf{m}_v , and we use a fixed total size $V = 20$ for each map element. We remain the original manhattan distance loss \mathbf{L}_{mht} [24] with hyper-parameters λ_1 and λ_2 to balance the convergence ability and the element accuracy.

Pose Auxiliary Loss. Given a coarse initial pose \mathbf{T}^0 , the \mathbf{Q}_{map} of the input prior-map may be incorrectly positioned. Hence, the pose auxiliary loss \mathbf{L}_{pose} is designed to provide additional supervision for the transformer decoder, helping it learn to correct such misalignment more effectively. Our end-to-end design utilizes the output features from the decoder to precisely align perceived map elements with the prior-map. Regarding map alignment, information can be retrieved with in the map queries \mathbf{Q}_{map} , which are then added to the output of each decoder layer. Subsequently, we utilize a shared MLP and a max-pooling layer to obtain the predicted delta pose $\partial\hat{\mathbf{T}}_{\text{aux}}$. Finally, the predicted delta pose is supervised by ground truth delta pose $\partial\mathbf{T}$ with a smooth L1 Loss.

3.5. MAP for Localization and Crowdsourcing

Optimization-based Localization. For the $\text{Localize}(\cdot)$ operation, we can explicitly remove map-changing events $\Delta_t \triangleq \{\mathbf{M}_t^{\text{F}}, \mathbf{M}_t^{\text{N}}\}$ from the matched associations $\mathbf{D}_t : \langle \mathbf{M}_t^{\text{M}}, \mathcal{M}_{t-1} \rangle$ for outlier rejection, and employ the additional probabilistic density of vertices \mathbf{U}_t . Specifically, we launch the following maximum a posteriori (MAP) state estimation for solving the vehicle pose:

$$\begin{aligned} &\min_{\mathbf{T}^{\text{R}}} \mathbf{E}^1(\mathbf{D}_t), \\ \mathbf{f}^1 &\propto \exp\left(-\frac{1}{2} \|\mathbf{T}^{\text{R}} \cdot \mathbf{m}_t^i - m_{t-1}^i\|_{\mathbf{g}_t^i}^2\right), \end{aligned} \quad (4)$$

where $\mathbf{E}^1(\mathbf{D}_t) = \sum_{\mathbf{D}_t} -\log(\mathbf{f}^1)$ is the sum of the negative log-likelihood of point-to-point residuals \mathbf{f}^1 , and we use the squared Mahalanobis distance whose covariance is assigned as the Gaussian mixture $\mathbf{g}_t^i \triangleq \mathbf{u}_t^i \oplus u_{t-1}^i$ of both inferred and crowdsourced probabilistic densities [5]. Each

pair of associations denoted as $d_t^i : \langle \mathbf{m}_t^i, m_{t-1}^i \rangle \in \mathbf{D}_t$ constructs a residual between corresponded vertices across two maps. One can combine more residuals like IMU pre-integration [11] or odometry [29, 41] for a tightly coupled system, and in this paper, we mainly test the difference between the single residual form \mathbf{E}^1 and the end-to-end regressed pose \mathbf{T}^{E} .

Probabilistic-aware Crowdsourcing. For the $\text{CSrc}(\cdot)$ operated on-the-cloud, we gather multi-traversal and multi-frame observations $\langle \mathbf{M}_t^j, \mathbf{U}_t^j, \mathbf{D}_t^j \rangle$ with their relative pose w.r.t. a base frame as \mathbf{T}_t^j , to fuse the crowdsourced map again in a MAP manner. For each tracked map vertex with multiple observations, we use the union-find algorithm to construct the following position solver for its latest position $m_t \in \mathcal{M}_t$:

$$\min_{m_t} \sum_{\hat{\mathbf{m}}_t^j \in \mathbf{M}} \frac{1}{2} \|m_t - \mathbf{T}_t^j \cdot \hat{\mathbf{m}}_t^j\|_{\mathbf{u}_t^j}^2 + \frac{1}{2} \|m_t - m_{t-1}\|_{u_{t-1}}^2, \quad (5)$$

where $\hat{\mathbf{m}}_t^j$ represents an associated observation \mathbf{M}_t^j , and the union \mathbf{M} gathers all matched observations, and we again use the Gaussian mixture model to continuously refine the probabilistic density u_t for each vertex. Meanwhile, we perform Hungarian voting to determine the predecessor and successor vertices of each vertex, to preserve the topology of HD map elements. For the first traverse, the second term leveraging the previous crowdsourced version is omitted for an initial crowdsourcing.

4. Implementation, Results, and Evaluation

4.1. Implementation details.

Training Sample Generation. To better align with real-world scenarios and improve the robustness of the network, we first apply random perturbations to the ground truth pose \mathbf{T}^{gt} to generate a noisy initial pose estimate \mathbf{T}^{init} . Based on \mathbf{T}^{init} , we then crop out the ground truth prior-map. Occasionally, when the local map obtained from the noisy pose is the same size as the perceptual range, some map elements may fall outside the perceptible area. To address this, we add padding to the perceptual range to ensure that all elements of the ground truth map remain within the perceptible region. Following this, we randomly remove certain elements from the prior-map and generate synthetic fake map elements. We do not perturb the ground truth map elements to simulate specific changes (such as shifting lane markings), as such modifications could be interpreted as deleting the original map elements and adding new ones.

Implementation and Training Details. We choose ResNet50 [13] as the image backbone. Our RTMap model is trained using 8 NVIDIA GeForce RTX 3090 GPUs with a total batch size of 32 for 36 epochs. We utilize the AdamW optimizer with a learning rate of 6×10^{-4} . To ensure fair

comparisons, we adopt the same training settings for MapTRv2 [24] and ensure its convergence. For \mathbf{L}_{pts} in Eq. 3, we set $\lambda_1 = 0.03$ and $\lambda_2 = 5.0$ for balancing their influence. For \mathbf{L}_{pose} , the translation weight is set to 0.04, corresponding to the scale in radians used when predicting the heading angle. We set the longitudinal range to $[-36, 36]$ and the lateral range to $[-18, 18]$ meters for online HD mapping.

4.2. Experiment Setup

Datasets. We evaluate the performance of the proposed network using two datasets: TbV [17] and nuScenes [3]. The TbV dataset [17] provides over 200 scenarios involving real-world changes. These map-changing events are primarily on lane topology, road boundaries, and pedestrian crossings. It is specifically designed to detect discrepancies between sensor data and HD maps caused by these changes, with the val set containing scenarios that feature actual map alterations. For training, the dataset also incorporates synthetically modified ground truth maps. The nuScenes dataset [3] is a large-scale dataset for autonomous driving, consisting of 1,000 driving scenes in urban environments, each sampled at 2Hz. It includes sensor data such as RGB images, LiDAR point clouds, inertial measurements, and labeled HD maps for evaluation.

Tasks and Metrics. Regarding the sufficiency of multi-traversal scanning and map-changing events, we test all sub-tasks, including crowdsourcing, change detection, and localization on the TbV dataset. Meanwhile, we use the nuScenes dataset to test the performance of our map-based localization w.r.t. its labeled HD map.

For the crowdsourced mapping task, we maintain the evaluation method used in online HD mapping tasks to assess the mapping results compared to single-traversal methods. To obtain ground truth for evaluation, we augment the map data by aligning the previous validation set with sensor data for ensuring 3D consistency. Specifically, we use average precision to evaluate the quality of the generated map and Chamfer distance to determine the alignment between the ground truth and predicted maps. We compute the AP at the following thresholds $\{0.5, 1.0, 1.5\}$ in meters keeping the same with experiments in other methods [24], and then calculate the mean to obtain the final mean average precision (mAP).

For the change detection task, we follow the evaluation implementation of the officially released code in TbV [17], to treat the change detection task as a binary classification problem (Acc), with classes indicating whether a change has occurred Acc_c or not Acc_r , and the mean accuracy ($mAcc$) is also calculated to assess overall performance.

For the localization task, we measure the mean and 90th absolute error of ego-poses relative to the ground truth HD

map in three main dimensions: lateral, longitudinal, and yaw.

4.3. Performance on Crowdsourcing

We cluster multi-traversal spatially overlapped driving clips in TbV for performing crowdsourcing, group 15 found clips into two scenarios – straight (6) and turning (9), and listed our results in comparison to our baseline MapTRv2 [24] as in Tab. 1. While single-traversal methods perform consistently among different cycles, our crowdsourced mapping framework gradually improves the prior-aided map quality through multiple cycles. We also compare to a direct version, which does not infer and use probabilistic densities \mathbf{U} during crowdsourcing, highlighting the effectiveness of leveraging such uncertainty in mapping tasks. We also refer readers to Fig. 4, which presents the trend of quality improvement by solving a precise trajectory and experiencing multi-traversals.

Table 1. Quantitative comparison of different online mapping approaches and strategies on TbV [17]. We additionally perform an ablation study on whether or not to use the vertex-level probabilistic density for crowdsourcing.

Method	Cycle	mAP(%) \uparrow			Avg.
		Ped.	Div.	Bou.	
Straight					
MapTRv2	Ave.	31.7	42.0	37.3	37.1
Ours (w/o \mathbf{U})	2	28.6	60.5	31.7	40.2
Ours	2	32.7	68.6	35.5	45.6
Ours (w/o \mathbf{U})	3	35.7	74.4	42.0	50.7
Ours	3	40.9	84.3	47.6	57.6
Turning					
MapTRv2	Ave.	28.2	31.6	18.3	26.0
Ours (w/o \mathbf{U})	2	30.2	65.5	30.1	41.9
Ours	2	33.1	71.0	32.3	45.5
Ours (w/o \mathbf{U})	3	35.9	71.2	32.6	46.5
Ours	3	42.3	85.2	38.8	55.4

4.4. Performance on Change Detection

To evaluate the effectiveness of the proposed RTMap under dynamic driving conditions, we performed change detection tests on the TbV dataset, with modifications including ‘insert crosswalk’ and ‘delete crosswalk’.

The results of our experiments, presented in Tab. 2, indicate a clear distinction in performance across the different scenarios, with our model demonstrating a particularly high sensitivity to the ‘changed’ category. This suggests that RTMap is well-suited to recalling possible map-changing events. Practically, a higher recall enables crowd-mining on these dubious events and ensures safety. Nevertheless, our

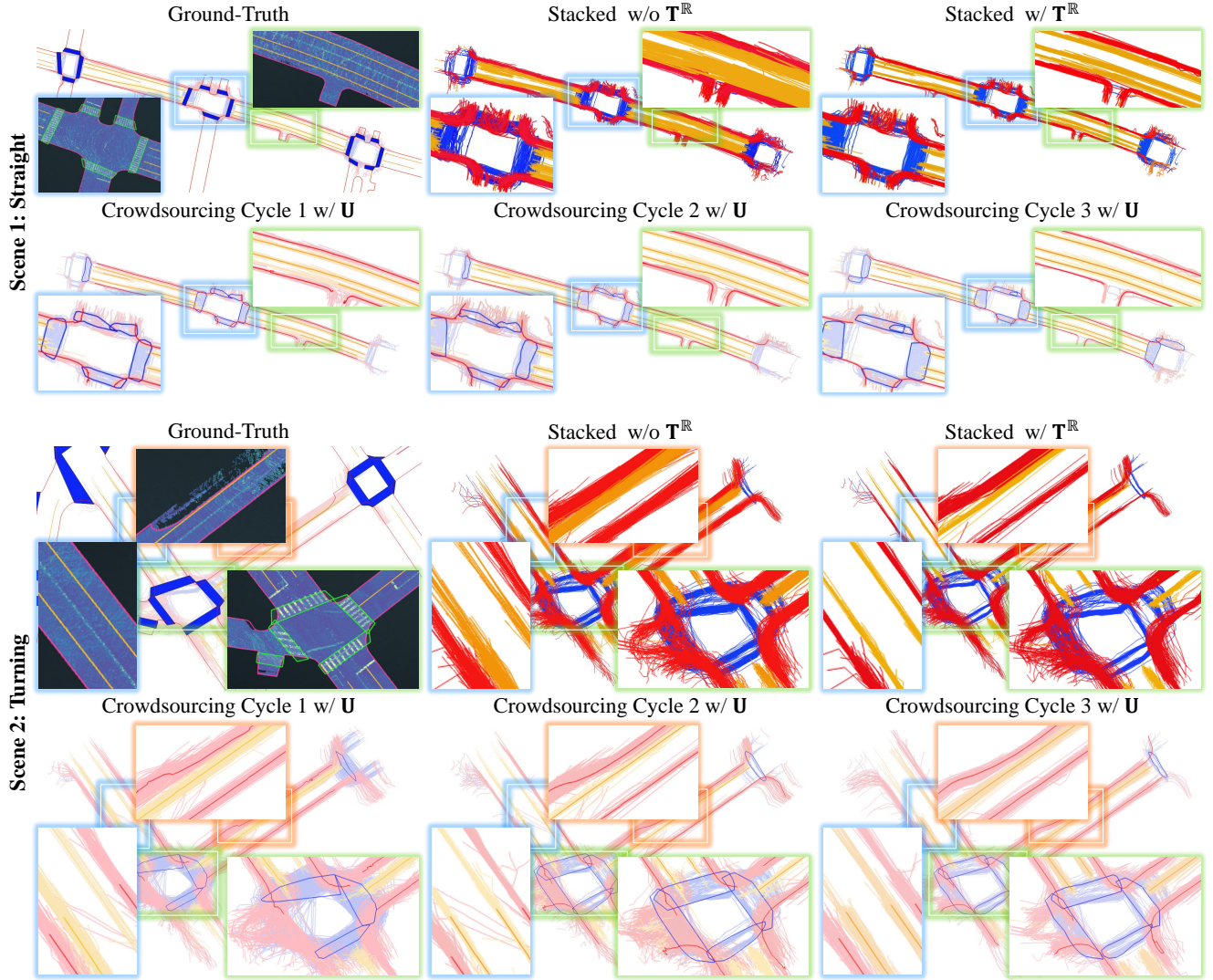


Figure 4. Qualitative comparison trending the quality improvement through solving a precise pose for alignment, and a multi-traversal probabilistic-aware crowdsourced HD mapping. We zoom-in several map regions for further comparisons.

method achieves higher overall accuracy than the previous method.

From the results, we can conclude that the RTMap’s performance is robust in dynamic contexts. This capability not only enhances the model’s effectiveness but also indicates its potential applicability in real-world scenarios, where rapid adaptation to environmental changes is essential.

4.5. Performance on Localization

Our end-to-end framework also supports localizing the vehicle w.r.t. the prior-map. In the first experiment, we perform an ablation study on whether or not to incorporate the change detection task – differentiating Q_{map} from Q_{prior} , and show the results in Tab. 3 and Fig. 5-(b), which proves

Table 2. Quantitative comparison of change detection between ours and the original approach proposed for TbV [17].

Method	$Acc_c(\%) \uparrow$	$Acc_r(\%) \uparrow$	$mAcc(\%) \uparrow$
TbV [17]	40.0	68.2	54.1
RTMap	48.9	66.0	57.4

the advantage of tightly coupling the change detection task to reject mismatched map elements for localization.

We also evaluate localization on the nuScenes dataset as listed in Tab. 4, which includes 100 different scenarios from the validation set. We find the following conclusions through experimental results: (1) The explicit optimization-

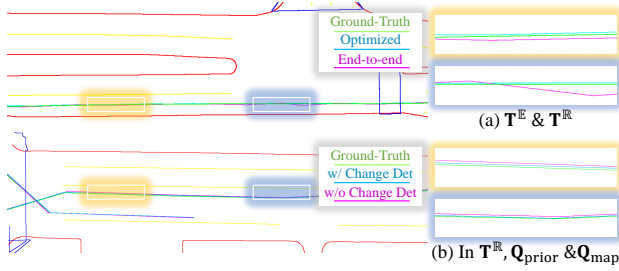


Figure 5. Qualitative comparison of the localization performance between two configurations on TbV [17], we show deviations of our estimated trajectory w.r.t. the ground truth, to illustrate the effectiveness of leveraging state optimization (\mathbf{T}^{R}) and map changing events (\mathbf{Q}_{map}) for further improving the accuracy.

Table 3. An ablation on whether or not using hybrid queries to distinguish \mathbf{Q}_{fake} from \mathbf{Q}_{map} on TbV [17].

Method	Lat (m)↓		Lon (m)↓		Yaw (°)↓	
	Mean	90 th	Mean	90 th	Mean	90 th
RTMap ($\mathbf{Q}_{\text{prior}}$)	0.163	0.318	0.686	1.616	0.332	0.766
RTMap (\mathbf{Q}_{map})	0.125	0.256	0.633	1.530	0.317	0.713

based pose estimation \mathbf{T}^{R} still outperforms the end-to-end manner \mathbf{T}^{E} , (2) the proposed loss functions in Sec. 3.4, including the localization loss \mathbf{L}_{pose} and the probabilistic density aware vertex regression loss \mathbf{L}_{pts} during training, can effectively contribute to the localization task.

In the current framework, we no longer require a standalone map-based localization task [14, 40] to serve downstream planning and control modules. Instead, we concentrate on tightly coupling change detection, localization, and the prior-map together, to benefit the completeness and robustness of the local map for serving downstream planning and control modules.

Table 4. Ablations of accuracy between end-to-end pose estimation \mathbf{T}^{E} , and optimization-based pose estimation \mathbf{T}^{R} under different settings on nuScenes [3].

Method	Lat (m)↓		Lon (m)↓		Yaw (°)↓	
	Mean	90 th	Mean	90 th	Mean	90 th
RTMap (\mathbf{T}^{E})	0.142	0.306	0.589	1.447	0.521	1.091
RTMap (\mathbf{T}^{R})	0.121	0.257	0.586	1.429	0.368	0.799
\mathbf{T}^{R} : Base	0.122	0.254	0.618	1.510	0.390	0.840
\mathbf{T}^{R} : + \mathbf{L}_{pose}	0.122	0.261	0.590	1.436	0.371	0.800
\mathbf{T}^{R} : + \mathbf{L}_{pts}	0.118	0.242	0.609	1.507	0.376	0.841

5. Conclusion

We presented RTMap, an end-to-end framework for real-time crowdsourcing mapping. Integrating prior-aided localization, change detection, and multi-agent crowdsourcing. Its functionality includes: (1) a multi-task architecture deployed onboard for concurrently performing localization, map change detection, vectorized HD mapping, reaching real-time performance on robust HD map servicing, (2) uncertainty-aware modeling, which probabilistically represents element uncertainties to improve localization accuracy and map quality, and (3) crowdsourced mapping, enabling continuous global map refinement via collaborative multi-agent multi-traversal data. Experiments on TbV and nuScenes datasets have demonstrated RTMap’s performance for all these tasks, with dynamic updates ensuring temporal consistency. By bridging onboard perception and asynchronous cloud computing, RTMap advances safe, adaptive autonomous driving solutions to maintain and leverage a self-evolutional memory.

Future work. Our future directions include incorporating more sensors (e.g., LiDAR) to form a multi-modal sensor fusion and uploading auxiliary but highly compact data for better probabilistic modeling on the cloud. Expanding validation to unstructured terrains and more complex urban environments will better establish the framework’s generalizability.

Acknowledgements

We thank the reviewers for the valuable discussions. We respect to our past and present colleagues for their unwavering dedication to pursuing innovative lighter-map solutions, whose contributions have profoundly bring-up this work. This research was supported by the Zhejiang Provincial Natural Science Foundation of China under Grant No. LD24F030001.

References

- [1] Samuel M Bateman, Ning Xu, H Charles Zhao, Yael Ben Shalom, Vince Gong, Greg Long, and Will Maddern. Exploring real world map change generalization of prior-informed hd map prediction models. In *CVPR*, pages 4568–4578, 2024. 2
- [2] Sean L. Bowman, Nikolay Atanasov, Kostas Daniilidis, and George J. Pappas. Probabilistic data association for semantic SLAM. In *ICRA*, pages 1722–1729, 2017. 3
- [3] Holger Caesar, Varun Bankiti, Alex H Lang, Sourabh Vora, Venice Erin Liong, Qiang Xu, Anush Krishnan, Yu Pan, Giancarlo Baldan, and Oscar Beijbom. nuScenes: A multimodal dataset for autonomous driving. In *CVPR*, pages 11621–11631, 2020. 2, 6, 8
- [4] Andrea Boscolo Camilletto, Alfredo Bochicchio, Alexander Liniger, Dengxin Dai, and Abel Gawel. U-bev: Height-

- aware bird's-eye-view segmentation and neural map-based relocalization. In *IROS*, pages 5597–5604, 2024. 2
- [5] Yan-Pei Cao, Leif Kobbelt, and Shi-Min Hu. Real-time high-accuracy three-dimensional reconstruction with consumer rgb-d cameras. *ACM TOG*, 37(5):171:1–171:16, 2018. 3, 5
- [6] Jiagang Chen, Liangliang Pan, Shunping Ji, Ji Zhao, and Zichao Zhang. Online temporal fusion for vectorized map construction in mapless autonomous driving. *arXiv:2409.00593*, 2024. 2
- [7] Shaoyu Chen, Tianheng Cheng, Xinggong Wang, Wenming Meng, Qian Zhang, and Wenyu Liu. Efficient and robust 2d-to-bev representation learning via geometry-guided kernel transformer. *arXiv:2206.04584*, 2022. 2
- [8] Wentao Cheng, Sheng Yang, Maomin Zhou, Ziyuan Liu, Yiming Chen, and Mingyang Li. Road mapping and localization using sparse semantic visual features. *IEEE Robotics and Automation Letters*, 6(4):8118–8125, 2021. 3
- [9] Zheng-Jun Du, Shi-Sheng Huang, Tai-Jiang Mu, Qunhe Zhao, Ralph R Martin, and Kun Xu. Accurate dynamic slam using crf-based long-term consistency. *IEEE TVCG*, 28(4):1745–1757, 2020. 3
- [10] Gamal Elghazaly, Raphaël Frank, Scott Harvey, and Stefan Saffko. High-definition maps: Comprehensive survey, challenges and future perspectives. *IEEE Open Journal of Intelligent Transportation Systems*, 4:527–550, 2023. 2
- [11] Christian Forster, Luca Carlone, Frank Dellaert, and Davide Scaramuzza. On-manifold preintegration for real-time visual-inertial odometry. *IEEE Transactions on Robotics*, 33(1):1–21, 2016. 5
- [12] Xunjiang Gu, Guanyu Song, Igor Gilitschenski, Marco Pavone, and Boris Ivanovic. Producing and leveraging online map uncertainty in trajectory prediction. In *CVPR*, pages 14521–14530, 2024. 3, 4
- [13] Kaiming He, Xiangyu Zhang, Shaoqing Ren, and Jian Sun. Deep residual learning for image recognition. In *CVPR*, pages 770–778, 2016. 5
- [14] Yuzhe He, Shuang Liang, Xiaofei Rui, Chengying Cai, and Guowei Wan. Egovm: Achieving precise ego-localization using lightweight vectorized maps. *arXiv:2307.08991*, 2023. 2, 3, 8
- [15] Shi-Sheng Huang, Ze-Yu Ma, Tai-Jiang Mu, Hongbo Fu, and Shi-Min Hu. Lidar-monocular visual odometry using point and line features. In *ICRA*, pages 1091–1097, 2020. 3
- [16] Zhou Jiang, Zhenxin Zhu, Pengfei Li, Huan-ang Gao, Tianyuan Yuan, Yongliang Shi, Hang Zhao, and Hao Zhao. P-MapNet: Far-seeing map generator enhanced by both sdmap and hdmap priors. In *ICLR*, pages 1–12, 2024. 2
- [17] John Lambert and James Hays. Trust, but verify: Cross-modality fusion for hd map change detection. In *NeurIPS*, pages 1–14, 2021. 2, 6, 7, 8
- [18] Dongjae Lee, Minwoo Jung, Wooseong Yang, and Ayoung Kim. Lidar odometry survey: recent advancements and remaining challenges. *Intelligent Service Robotics*, 17(2):95–118, 2024. 3
- [19] Qi Li, Yue Wang, Yilun Wang, and Hang Zhao. Hdmapnet: An online hd map construction and evaluation framework. In *ICRA*, pages 4628–4634, 2022. 2
- [20] Siyu Li, Jiacheng Lin, Hao Shi, Jiaming Zhang, Song Wang, You Yao, Zhiyong Li, and Kailun Yang. DTCLMapper: Dual temporal consistent learning for vectorized hd map construction. *arXiv:2405.05518*, 2024. 2
- [21] Tianyu Li, Peijin Jia, Bangjun Wang, Li Chen, Kun Jiang, Junchi Yan, and Hongyang Li. LaneSegNet: Map learning with lane segment perception for autonomous driving. In *ICLR*, 2024. 2
- [22] Zhiqi Li, Wenhai Wang, Hongyang Li, Enze Xie, Chonghao Sima, Tong Lu, Yu Qiao, and Jifeng Dai. BEVFormer: Learning bird's-eye-view representation from multi-camera images via spatiotemporal transformers. In *ECCV*, pages 1–18, 2022. 2
- [23] Bencheng Liao, Shaoyu Chen, Xinggong Wang, Tianheng Cheng, Qian Zhang, Wenyu Liu, and Chang Huang. MapTR: Structured modeling and learning for online vectorized hd map construction. In *ICLR*, pages 1–18, 2023. 1, 2, 3, 4
- [24] Bencheng Liao, Shaoyu Chen, Yunchi Zhang, Bo Jiang, Qian Zhang, Wenyu Liu, Chang Huang, and Xinggong Wang. MapTRv2: An end-to-end framework for online vectorized hd map construction. *arXiv:2308.05736*, 2023. 2, 5, 6
- [25] Xiaolu Liu, Song Wang, Wentong Li, Ruizi Yang, Junbo Chen, and Jianke Zhu. MGMap: Mask-guided learning for online vectorized hd map construction. In *CVPR*, pages 14812–14821, 2024. 1, 2
- [26] Yicheng Liu, Tianyuan Yuan, Yue Wang, Yilun Wang, and Hang Zhao. VectorMapNet: End-to-end vectorized hd map learning. In *ICML*, pages 22352–22369, 2023. 2
- [27] Katie Luo, Xinchuo Weng, Yan Wang, Shuang Wu, Jie Li, Kilian Q Weinberger, Yue Wang, and Marco Pavone. Augmenting lane perception and topology understanding with standard definition navigation maps. In *ICRA*, pages 4029–4035, 2024. 2
- [28] Jinyu Miao, Kun Jiang, Tuopu Wen, Yunlong Wang, Peijin Jia, Benny Wijaya, Xuhe Zhao, Qian Cheng, Zhongyang Xiao, Jin Huang, et al. A survey on monocular relocalization: From the perspective of scene map representation. *IEEE TIV*, pages 1–33, 2024. 3
- [29] Tong Qin, Peiliang Li, and Shaojie Shen. Vins-mono: A robust and versatile monocular visual-inertial state estimator. *IEEE Transactions on Robotics*, 34(4):1004–1020, 2018. 5
- [30] Tong Qin, Changze Li, Haoyang Ye, Shaowei Wan, Minzhen Li, Hongwei Liu, and Ming Yang. Crowd-sourced nerf: Collecting data from production vehicles for 3d street view reconstruction. *IEEE Transactions on Intelligent Transportation Systems*, 25(11):16145–16156, 2024. 2
- [31] Rémy Sun, Li Yang, Diane Lingrand, and Frédéric Precioso. Mind the map! accounting for existing map information when estimating online hdmaps from sensor data. In *WACV*, pages 1–11, 2025. 2, 3, 4
- [32] Kun Tang, Xu Cao, Zhipeng Cao, Tong Zhou, Erlong Li, Ao Liu, Shengtao Zou, Chang Liu, Shuqi Mei, Elena Sizikova, et al. THMA: Tencent hd map ai system for creating hd map annotations. In *AAAI*, pages 15585–15593, 2023. 2
- [33] Benny Wijaya, Kun Jiang, Mengmeng Yang, Tuopu Wen, Yunlong Wang, Xuewei Tang, Zheng Fu, Taohua Zhou, and Diange Yang. High definition map mapping and update: A

general overview and future directions. *arXiv:2409.09726*, 2024. 1, 2

- [34] Lena Wild, Ludvig Ericson, Rafael Valencia, and Patric Jensfelt. Exelmap: Explainable element-based hd-map change detection and update. *arXiv:2409.10178*, 2024. 3
- [35] Chenming Wu, Jiadai Sun, Zhelun Shen, and Liangjun Zhang. MapNeRF: Incorporating map priors into neural radiance fields for driving view simulation. In *IROS*, pages 7082–7088, 2023. 2
- [36] Deguo Xia, Weiming Zhang, Xiyan Liu, Wei Zhang, Chenting Gong, Xiao Tan, Jizhou Huang, Mengmeng Yang, and Diange Yang. LDMapNet-U: An end-to-end system for city-scale lane-level map updating. In *KDD*, 2025. 3
- [37] Xuan Xiong, Yicheng Liu, Tianyuan Yuan, Yue Wang, Yilun Wang, and Hang Zhao. Neural map prior for autonomous driving. In *CVPR*, pages 17535–17544, 2023. 2
- [38] Sheng Yang, Xiaoling Zhu, Xing Nian, Lu Feng, Xiaozhi Qu, and Teng Ma. A robust pose graph approach for city scale LiDAR mapping. In *IROS*, pages 1175–1182, 2018. 2
- [39] Tianyuan Yuan, Yicheng Liu, Yue Wang, Yilun Wang, and Hang Zhao. StreamMapNet: Streaming mapping network for vectorized online hd map construction. In *WACV*, pages 7341–7350, 2024. 2
- [40] Zhihuang Zhang, Meng Xu, Wenqiang Zhou, Tao Peng, Liang Li, and Stefan Poslad. Bev-locator: An end-to-end visual semantic localization network using multi-view images. *arXiv:2211.14927*, 2022. 3, 8
- [41] Bin Zhao, Yunzhou Zhang, Junjie Huang, Xichen Zhang, Zeyu Long, and Yulong Li. L-VIWO: Visual-inertial-wheel odometry based on lane lines. In *ICRA*, pages 18079–18085, 2024. 3, 5
- [42] Zi-Xin Zou, Shi-Sheng Huang, Yan-Pei Cao, Tai-Jiang Mu, Ying Shan, Hongbo Fu, and Song-Hai Zhang. GP-Recon: Online monocular neural 3d reconstruction with geometric prior. *IEEE TVCG*, 2024. 3